




# A 1536-Well Quantitative High-Throughput Screen to Identify Compounds Targeting Cancer Stem Cells

Journal of Biomolecular Screening  
17(9) 1231–1242  
© 2012 Society for Laboratory  
Automation and Screening  
DOI: 10.1177/1087057112458152  
<http://jbx.sagepub.com>  


Lesley A. Mathews<sup>1</sup>, Jonathan M. Keller<sup>1</sup>, Bonnie L. Goodwin<sup>1</sup>,  
Rajarshi Guha<sup>1</sup>, Paul Shinn<sup>1</sup>, Rebecca Mull<sup>1</sup>, Craig J. Thomas<sup>1</sup>,  
Rachel L. de Kluyver<sup>2</sup>, Thomas J. Sayers<sup>3</sup>, and Marc Ferrer<sup>1</sup>

## Abstract

Tumor cell subpopulations called cancer stem cells (CSCs) or tumor-initiating cells (TICs) have self-renewal potential and are thought to drive metastasis and tumor formation. Data suggest that these cells are resistant to current chemotherapy and radiation therapy treatments, leading to cancer recurrence. Therefore, finding new drugs and/or drug combinations that cause death of both the differentiated tumor cells as well as CSC populations is a critical unmet medical need. Here, we describe how cancer-derived CSCs are generated from cancer cell lines using stem cell growth media and nonadherent conditions in quantities that enable high-throughput screening (HTS). A cell growth assay in a 1536-well microplate format was developed with these CSCs and used to screen a focused collection of oncology drugs and clinical candidates to find compounds that are cytotoxic against these highly aggressive cells. A hit selection process that included potency and efficacy measurements during the primary screen allowed us to efficiently identify compounds with potent cytotoxic effects against spheroid-derived CSCs. Overall, this research demonstrates one of the first miniaturized HTS assays using CSCs. The procedures described here should enable further testing of the effect of compounds on CSCs and help determine which pathways need to be targeted to kill them.

## Keywords

qHTS, cancer stem cells, pancreatic cancer, prostate cancer

## Introduction

The American Cancer Society estimated that more than 240 000 new cases of male prostate cancer were diagnosed in 2011, and 30 000 men will die due to this disease. Localized prostate cancer responds well to resection, chemotherapy, and radiation, but overall survival rates are low as a result of colonizing metastases. A lower number of Americans were diagnosed with pancreatic cancer in 2011 in the United States with 44 000 new patients,<sup>1</sup> yet the disease remains the fourth leading cause of cancer death overall. In the same year, 37 000 people were predicted to die as a result of this disease,<sup>1</sup> which is 85% of all diagnosed patients. Since 1975, the 5-year survival rate for pancreatic cancer has improved only from 3% to 6%, and in fact, pancreatic cancer is the only one of the top 10 cancer killers that still has a 5-year survival rate in the single digits. Surgical resection is the best method for long-term survival in patients, but only about 15% of the patients are diagnosed early enough to be eligible for surgery, and furthermore, 80% of those patients who will undergo surgery will

have a recurrence of the disease within 2 years.<sup>1</sup> This percentage remains high due to the aggressive nature of pancreatic cancer and the ability of highly invasive cells to resist current treatment regimes.<sup>2–4</sup>

<sup>1</sup>Division of Preclinical Innovation, National Center for Advancing Translational Sciences (NCATS), National Institutes of Health, Rockville, MD, USA

<sup>2</sup>Kolling Institute of Medical Research, Northern Clinical School, University of Sydney, NSW, Australia

<sup>3</sup>Basic Sciences Program, SAIC-Frederick, Inc., NCI Cancer and Inflammation Program, Frederick National Laboratory, Frederick, MD, USA

Received Apr 3, 2012, and in revised form Jun 11, 2012. Accepted for publication Jun 23, 2012.

Supplementary material for this article is available on the *Journal of Biomolecular Screening* Web site at <http://jbx.sagepub.com/supplemental>.

## Corresponding Author:

Lesley A. Mathews, National Institutes of Health, 9800 Medical Center Drive, Rockville MD 20850, USA  
Email: [mathewsla@mail.nih.gov](mailto:mathewsla@mail.nih.gov)

In both pancreatic and prostate cancers, highly invasive cells are able to survive and metastasize to other vital organs, which is uniformly fatal in patients.<sup>2</sup> A vast majority of the patients diagnosed with pancreatic cancer receive the nucleoside analogue drug gemcitabine as part of their treatment regime, and those with prostate cancer receive the cell cycle inhibitor docetaxel.<sup>5,6</sup> Recent evidence suggests that a small population of cells, referred to as tumor-initiating cells (TICs) or circulating tumor cells (CTCs), within a heterogeneous tumor have an enhanced capacity to form a tumor; are responsible for propagation, relapse, and metastatic dissemination; and are the root cause of patient resistance to treatment and ultimate death. However, because these tumor-initiating cells also possess certain stem cell-like properties (e.g., quiescence, self-renewal, asymmetric division, and multidrug resistance), permitting them to drive tumor growth and evade conventional therapies, they have also been called cancer stem cells (CSCs). To date, CSCs have been isolated from almost every solid tumor type.<sup>7–11</sup> In the past few years, CSCs have been isolated from cancers by fluorescence-activated cell sorting (FACS) selecting for expression of CD44, CD24, ESA, or CD133.<sup>12</sup> In addition, CSCs can be isolated by generating spheroids using specialized culture conditions and highly defined media called stem cell media (SCM).<sup>13–16</sup> The spheres express higher levels of the stem cell markers indicated above and demonstrate higher tumorigenic potential in animals compared with total cells.<sup>15,16</sup>

Because of the limited treatment options for aggressive types of many cancers, we sought to find compounds capable of killing the CSC populations in spheroid-derived model systems of the prostate and the pancreas.<sup>17</sup> Using a 1536-well microplate format and a cell growth assay, an in-house small-molecule collection consisting of compounds targeting oncology-relevant pathways/mechanisms of survival was screened. The screen was implemented by testing the compounds in dose-response format, which allowed for a hit selection process that included both potency and efficacy to efficiently identify compounds with potent cytotoxic effects for CSCs. A few compounds were able to inhibit the growth of the CSCs and the parental adherent cells from both cancer types with high potency and efficacy. The initial results were further validated in a functional assay of CSC invasion using Matrigel-coated Boyden chambers. Finally, we used a highly aggressive mouse breast cancer cell line, 4T1.2, which has been stably infected with a Nanog-GFP reporter as a model system to determine if compounds affected the “stemness” of the cells by measuring effects directly on a stem cell reporter. This research demonstrates one of the first quantitative high-throughput screening (qHTS)-based assays using nonengineered CSCs. Overall, the determination of which pathways need to be inhibited to produce toxicity against CSCs will result in the development of novel therapies for aggressive forms

of cancer and will specifically result in targeting metastasis and recurrence.

## Materials and Methods

**Cell lines and reagents.** PANC1 human pancreatic cancer and LNCaP human prostate cancer cell lines were obtained from ATCC (Manassas, VA) and cultured according to the manufacturer's instructions (Cell Line Verification Test Recommendations, ATCC Technical Bulletin No. 8 [2008]). The mouse breast cancer line 4T1.2 Nanog-GFP was provided by Dr. Thomas Sayers from NCI-Frederick (Frederick, MD) and were grown in RPMI + 10% fetal bovine serum (FBS) (see Supplemental Methods for its construction). SCM was prepared as previously described.<sup>18</sup> Salinomycin was purchased from Sigma (St. Louis, MO), and all other chemicals (bortezomib, CMP1, and CMP1-S) were purchased from Selleck (Houston, TX).

**Sphere formation assays.** LNCaP and PANC1 spheres were generated as previously described.<sup>18,19</sup> Additional information is available in the Supplemental Methods section.

**Proliferation assays.** Assays were conducted in sterile, tissue culture-treated 1536-well white solid-bottom plates (catalog number 789173-F; Greiner Bio-One, Monroe, NC). A total of 200 cells per well in 5  $\mu$ L of SCM + KO + ITS were seeded using a Multidrop Combi Reagent dispenser with a small pin cassette (Thermo Scientific, Fisher Scientific, Fair Lawn, NJ). Immediately after dispensing the cells, 23 nL compound solution in DMSO was transferred using a Kalypsys (San Diego, CA) pintoole. The plates were then covered with stainless steel Kalypsys lids and placed into an incubator at 37 °C, with 5% CO<sub>2</sub> and 95% relative humidity. The plates were incubated for 48 h, and then 3  $\mu$ L CellTiter-Glo reagent assay (Promega, Madison, WI) was added using a BioRAPTR (Beckman Coulter, Brea, CA). Plates were incubated for 30 min at room temperature and spun at 1000 rpm, and relative luminescence units (RLU) were quantified using a ViewLux (PerkinElmer, Waltham, MA).

**Mechanism Interrogation PlatE (MIPE) compound library.** The library used in these studies is an internal collection of 112 high-value small molecules known to modulate oncology targets, pathways, and phenotypes, referred to as the MIPE-oncology library (MIPE: Mechanism Interrogation PlatE) (see Supplemental Methods section for additional information, and a full list of compounds is available upon request).

**Quantitative high-throughput screen (qHTS).** For the screen, the MIPE library compounds were transferred to columns 5 to 48, and controls were added in columns 1 to 4 of the assay plate. Columns 1 and 2 contained plain DMSO, whereas columns 3 and 4 contained 2-mM solutions of the protease inhibitor bortezomib or the antibiotic salinomycin

in DMSO (final concentration 9  $\mu\text{M}$ ). Compounds were tested as dose responses starting at a stock concentration of 10 mM (final concentration 46  $\mu\text{M}$ ) in DMSO and diluted 3-fold, also with DMSO. The library was tested at 12 compound concentrations for qHTS as described previously.<sup>20</sup> Relative luminescence units for each well were normalized to the median RLUs from the DMSO control wells as 100% viability and median RLUs from the salinomycin or bortezomib control wells as 0% viability. Additional information is available in the Supplemental Methods section.

**Hit selection from qHTS.** Hits were selected based on two methods: (1) a single % viability parameter at the compound dose that produced maximum cell killing. A compound that produced  $\geq 70\%$  cell killing ( $\leq 30\%$  cell viability) at the dose that produced maximum killing was considered a hit. (2) Curve response class (CRC) classification from dose-response HTS, in which normalized data were fitted to four-parameter dose-response curves using a custom grid-based algorithm to generate a CRC score for each compound dose response.<sup>20,21</sup> CRC values of  $-1.1$ ,  $-1.2$ ,  $-2.1$ , and  $-2.2$  are considered high-quality hits; CRC values of  $-1.3$ ,  $-1.4$ ,  $-2.3$ ,  $-2.4$ , and  $-3$  are inconclusive hits; and a CRC value of 4 is for inactive compounds. See Supplemental Methods for additional information.

**Matrigel invasion assay.** Matrigel-coated 24-well inserts (8  $\mu\text{m}$  pore size) were purchased from BD Biosciences Clontech (Palo Alto, CA), and the assay was done as described previously.<sup>17</sup> A detailed assay protocol is available in the Supplemental Methods section.

**High-content imaging Nanog-GFP assay.** A 1536-well high-content assay to measure Nanog-GFP levels in 4T1.2 cells was developed using an ArrayScan VTI (Thermo Scientific). A detailed assay protocol is available in the Supplemental Methods section.

## Results

### Development of a 1536-Well Microplate CSC Proliferation Assay Using CellTiter-Glo

A major challenge to using cancer stem cells for drug discovery is their production in quantities that enable their testing for screening of compound libraries. Limited number of CSCs can be isolated from bulk cancer cell populations by sorting for specific cell surface stem cell antigens, including CD44, CD24, and CD133.<sup>7,8,22</sup> Alternatively, protocols have also been developed for the isolation of CSCs from cell lines forming spheroids by using stem cell-specific growth media and nonadherent surfaces. The spheroid technique affords for the production of large amounts of CSCs and therefore enables the availability of these cells for the use in HTS. In this work, we adapted previously described methods to obtain pancreatic and prostate CSC spheroids from cancer cell lines (Suppl.

**Table S1**). The pancreatic and prostate cancer CSCs spheroids, referred to as spheres, were grown from parental cell lines for 7 to 14 days in stem cell media and hydrogel-coated flasks to prevent cell adhesion (Suppl. Fig. S1A). A similar set of assay plates containing the adherent parental population of PANC1 and LNCaP cells was also tested in their normal growth media with 5% serum. In a previously conducted screen against breast CSCs, the antibiotic salinomycin was discovered to be a potent inhibitor of CSC cell survival.<sup>23</sup> Therefore, we conducted an initial experiment to determine if salinomycin could be used as a positive control for inducing cell death in our CSC proliferation assays. Our PANC1-derived spheres demonstrated an  $\text{IC}_{50}$  of 13  $\mu\text{M}$ , and a similar response against LNCaP spheres was observed at 9  $\mu\text{M}$  (Suppl. Fig. S1B). These values were similar to those obtained in the breast CSC study, where salinomycin inhibited HMLER cell growth with an  $\text{IC}_{50}$  of 4 to 8  $\mu\text{M}$ . In addition, we tested the ability of the protease inhibitor bortezomib to inhibit the growth of our spheroid CSCs in our 1536-well system based on recent evidence that it could inhibit the growth of CSCs generated from a mouse breast cancer model 4T1.2 labeled with green fluorescent protein (GFP) for the stem cell marker Nanog (Thomas Sayers, NCI-Frederick, personal communication, 2011). The  $\text{IC}_{50}$ s for bortezomib were 6 nM against PANC1 spheres and 23 nM against LNCaP spheres (Suppl. Fig. S1B). The assay window parameters for the LNCaP adherent cells grown in 1536 are shown in Supplemental Figure S1C and for spheres in Supplemental Figure S1D.

### Screening the MIPE of Oncology Pathway Compounds

The spheroid CSC 1536-well plate growth assay was used to screen the National Center for Advancing Translational Sciences (NCATS) MIPE library of small molecules, which consisted of 112 unique compounds targeting oncology-relevant pathways/mechanisms of survival. The compounds were tested at 12 doses, starting at 46  $\mu\text{M}$  and diluted 3-fold, for their effect on growth of both PANC1 and LNCaP cells, both grown as spheres (CSCs) and adherent cells (original parental cells from which CSCs were obtained). Results were analyzed using two methods: % viability (corresponding to the % viability at the compound dose that produced maximum killing) and curve fit to the compound dose responses to generate CRC scores (see Materials and Methods). Analysis of the results comparing the % viability parameters for the different cell types and growth conditions showed robust correlation ( $R^2 = 0.47$ ) between the effects of compounds on cells grown as spheres versus adherent cells (Fig. 1A). In contrast, we observed a lack of correlation ( $R^2 = -0.81$ ) between the activity of the compounds on LNCaP versus PANC1 cells (Fig. 1B), suggesting that the cancer type, rather than

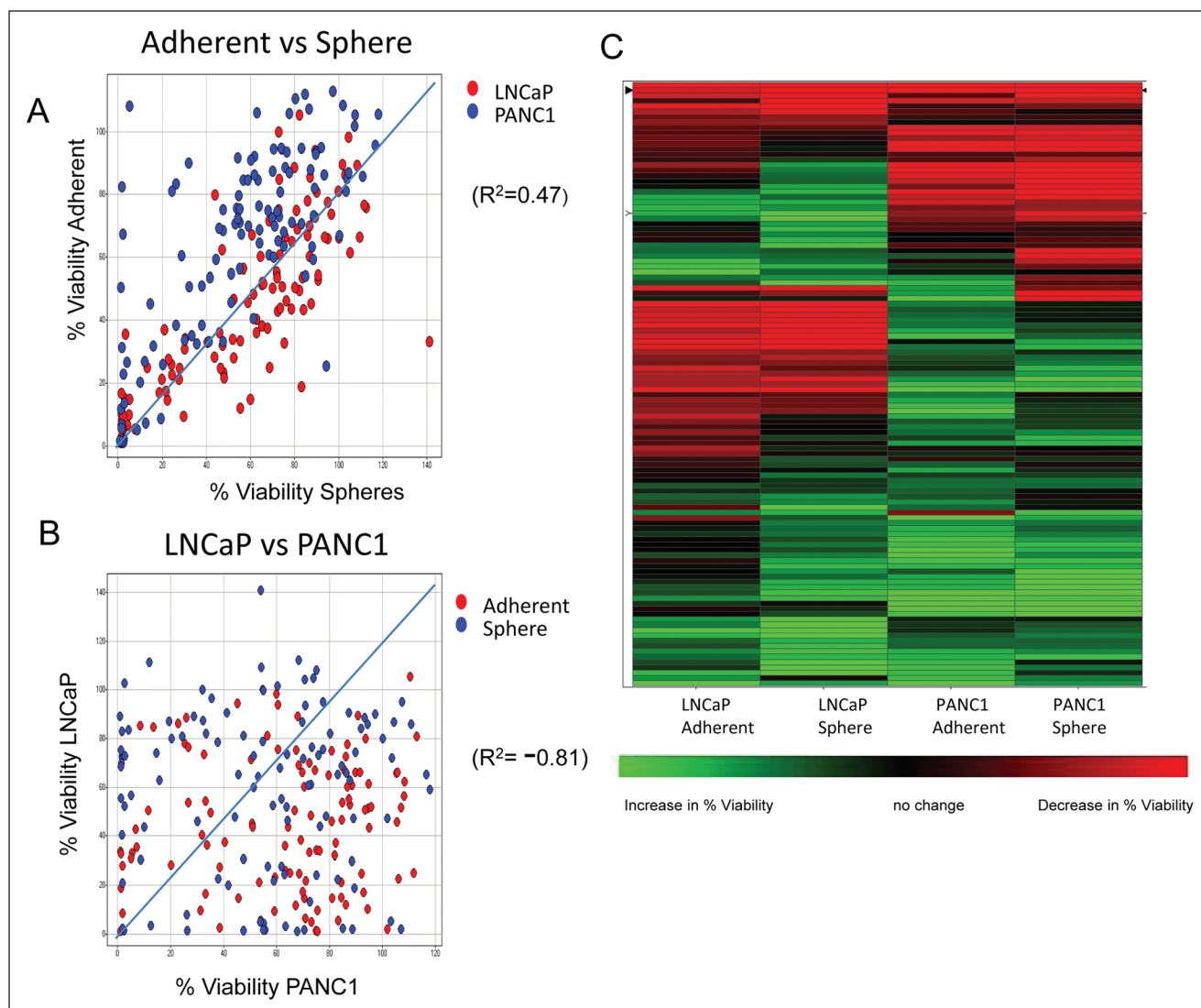


**Figure 1.** Results from quantitative high-throughput screening (qHTS) analyzed using % viability. **(A)** Correlation plots of % viability (normalized to DMSO-treated cells) between adherent versus sphere cells ( $R^2 = 0.47$ ) with LNCaP in red and PANC1 in blue. **(B)** Correlation plots of % viability normalized to DMSO-treated cells between LNCaP and PANC1 ( $R^2 = -0.81$ ) with adherent cells in red and spheres in blue. **(C)** Hierarchical clustering analysis of the % viability based on cancer type and growth condition demonstrates clusters of compounds that are pan-active in both LNCaP/PANC1 adherent/sphere-based cultures or active in LNCaP-adherent, LNCaP-sphere, PANC1-adherent, or PANC1-sphere. Red represents a decrease in viability, green is an increase, and black is no change. The % viability parameter from qHTS is the % viability at the compound dose that produced maximum cell killing.

growth mode, drove the differential cytotoxic effect of the compounds in the collection. A hierarchical clustering of the % viability values for the four different parameters is shown in **Figure 1C**. It again shows that clustering of compounds is driven mostly by the activity in cancer cell type, and most of the compounds are selective for their effect on either LNCaP or PANC1, regardless of whether the cells are grown as spheres or adherent cells. A small number of compounds are pan-active (meaning they were effective on both adherent cells and spheres and in both lines LNCaP and PANC1), and very few appear to be selective for just the

spheres (**Fig. 1C**). A stringent cutoff of  $\leq 30\%$  viability was chosen to select compounds as hits. This activity cutoff for hit selection was based on published data highlighting the resistance of CSCs to conventional therapies,<sup>24,25</sup> as well as based on the statistical parameters of the assay, especially for the sphere assay, where the mean  $-3$ \*standard deviation of the sample field for a DMSO plate was close to 30% viability (**Suppl. Fig. S1D**). Using the  $\leq 30\%$  viability cutoff, the hit rate for each screening condition was high, ranging from 20% to 50% (data not shown). This is not surprising because the collection is enriched for compounds

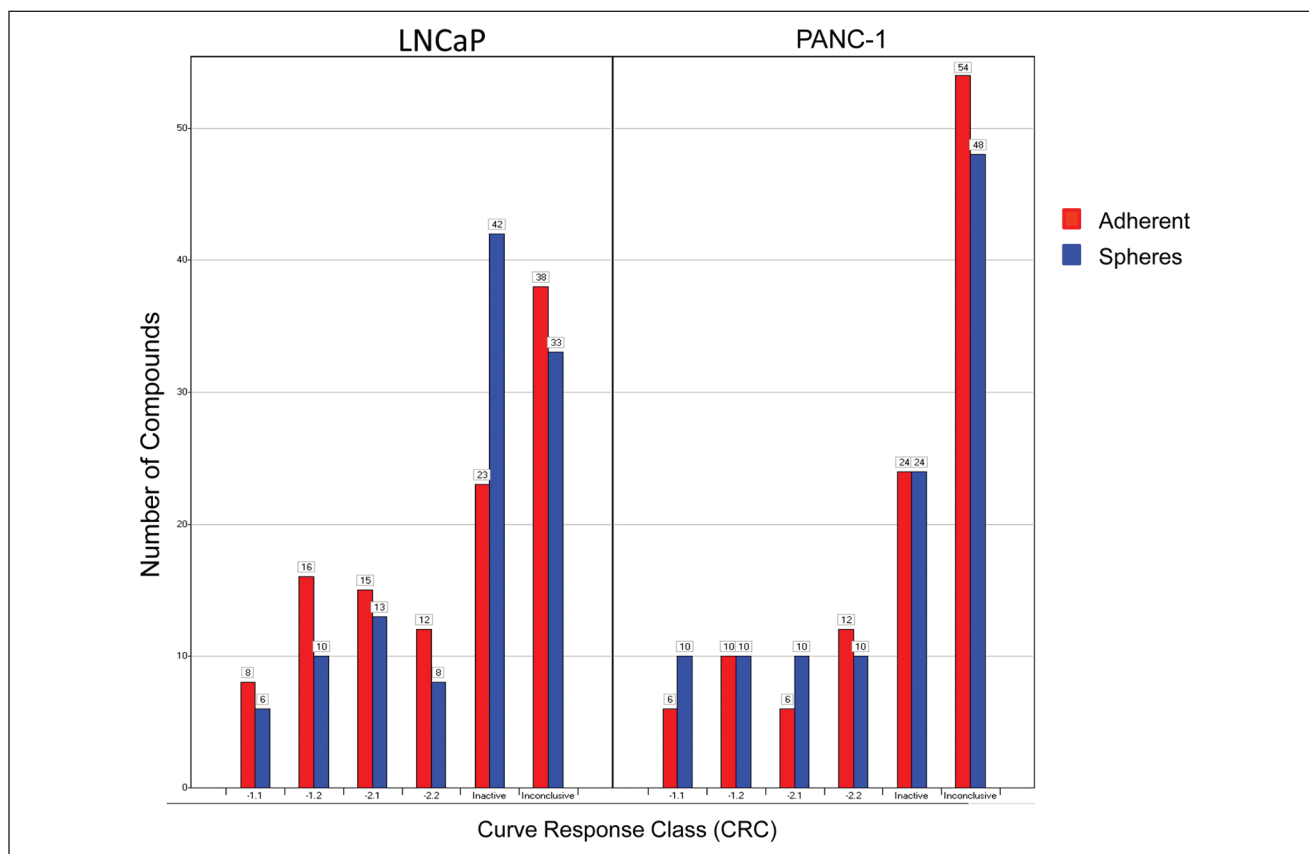


**Figure 2.** Results from quantitative high-throughput screening analyzed using curve response class (CRC) fitting, showing the CRC distribution of the number of compounds from both the LNCaP and PANC1 cell lines for both adherent (red) and sphere (blue) populations. CRCs  $-1.1$ ,  $-1.2$ ,  $-2.1$ , and  $-2.2$  are considered active, and CRC 4 is inactive. All other groups are clustered as inconclusive. A more detailed description of the CRCs can be found in the Supplemental Methods section and referenced in Inglesse et al.<sup>20</sup> and Wang et al.<sup>21</sup>

developed for cancer treatment. Although there was good overlap between hits in adherent versus sphere cells, the overlap between hits in LNCaPs versus PANC1 was small (Venn diagrams showing overlap between different conditions are shown in **Suppl. Fig. S2**), and only two unique compounds were identified to be pan-active in all four parameters (LNCaP-adherent, LNCaP-sphere, PANC1-adherent, PANC1-sphere).

A drawback of the traditional hit selection method based on a single % viability parameter to measure compound activity is that it selects compounds based mostly on efficacy and does not efficiently discern compounds based on potency. In this case, because the compounds were tested in dose responses, we were able to score each compound in dose response to a CRC,<sup>20</sup> which is a measure that includes potency, efficacy, and reliability of the data and estimates an  $IC_{50}$  value directly from the primary screen. Compounds that might look equally potent by % viability might in fact have a degree of selectivity that is only evident when comparing their CRCs and  $IC_{50}$  values. The distributions of

CRCs from the four parameters are shown in **Figure 2**. For the purposes of this study, we only considered active compounds those with high-quality curve classes ( $-1.1$ ,  $-1.2$ ,  $-2.1$ , and  $-2.2$ ). In general, the CRC distribution was very similar for both cell lines and growth conditions, suggesting that neither of the assay conditions tested was much more susceptible to compound treatment than the others. Any overlaps are visualized in Venn diagrams (**Suppl. Fig. S3**), as well as in the concordance matrices (**Suppl. Table S2**). Using CRC scoring, five compounds were identified as pan-active in both the cell lines and conditions (**Suppl. Fig. S3**). When comparing the hits from both selection methods, only one compound (CMP2) is selected by all methods. The dose-response curves and CRCs of CMP2 and two other compounds selected as pan-active by % viability (CMP1) and CRCs (CMP3) are shown in **Figure 3**. It is noteworthy to point out that although these compounds all met the hit selection criteria to be pan-active cytotoxic for both the prostate and pancreatic cancer cell lines and both growth conditions, adherent cells and spheres, the dose responses

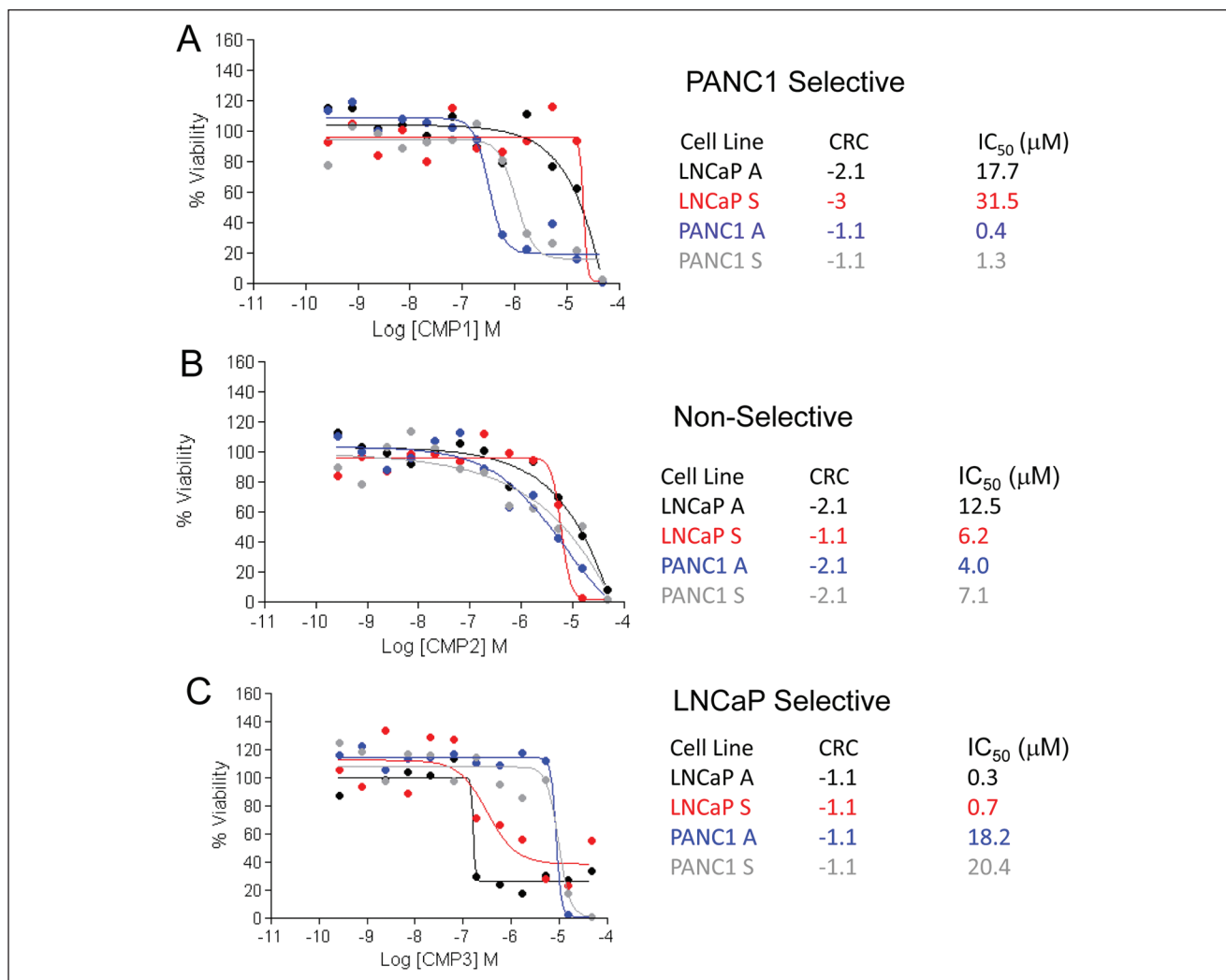


**Figure 3.** Dose-response curves of (A) CMP1, (B) CMP2, and (C) CMP3 with curve response class (CRC) score and predicted IC<sub>50</sub> values from the screen for cell proliferation in adherent LNCaP (black), LNCaP spheres (red), adherent PANC1 (blue), and PANC1 spheres (gray). Percent viability compared with DMSO control-treated cells appears on the y-axis and the log molar concentration on the x-axis. CMP1 was identified using the % viability method, CMP2 was identified using both % viability and CRCs, and CMP3 was identified by CRC analysis only.

indicate a certain degree of selectivity that is lost when just measuring % viability. For example, CMP2 appears equally potent in all assays (Fig. 3B), whereas CMP1 appears selective for PANC1 cells by more than 10-fold (Fig. 3A), and CMP3 appears selective for LNCaP cells by more than 10-fold (Fig. 3C). Also note that although not as dramatic, in most instances, a higher dose of compounds is required to kill the spheres compared with adherent cells. For example, the determined IC<sub>50</sub> for CMP1 was 18 μM for the LNCaP adherent cells but twice as high at 31 μM for the LNCaP spheres (Fig. 3A). Similarly, the IC<sub>50</sub> for the adherent PANC1 cells was 0.4 μM and was 3.5 times higher at 1.3 μM for the PANC1 spheres (Fig. 3A). To confirm the activity of CMP1, it was retested in a separate assay against spheres from PANC1 (Suppl. Fig. 4A) and from LNCaP

(Suppl. Fig. 4B). Bortezomib was also present in the MIPE library and was active against in both lines and populations (Suppl. Fig. 4C).

As discussed in the introduction, gemcitabine is the current standard of care treatment for pancreatic cancer. Gemcitabine is included in the MIPE collection and was therefore of interest to investigate the effect of this drug in the screen performed (Suppl. Fig. S5). The results show that gemcitabine was an efficacious (produces ~100% killing) but weak (estimated IC<sub>50</sub> ~50 μM) inhibitor of LNCaP cell viability, with similar effects in both adherent and sphere growth conditions. Gemcitabine was not efficacious at killing PANC1 cells in any of the growth conditions. At the highest dose tested, it only produced 40% killing. Although gemcitabine is the standard of care used to treat

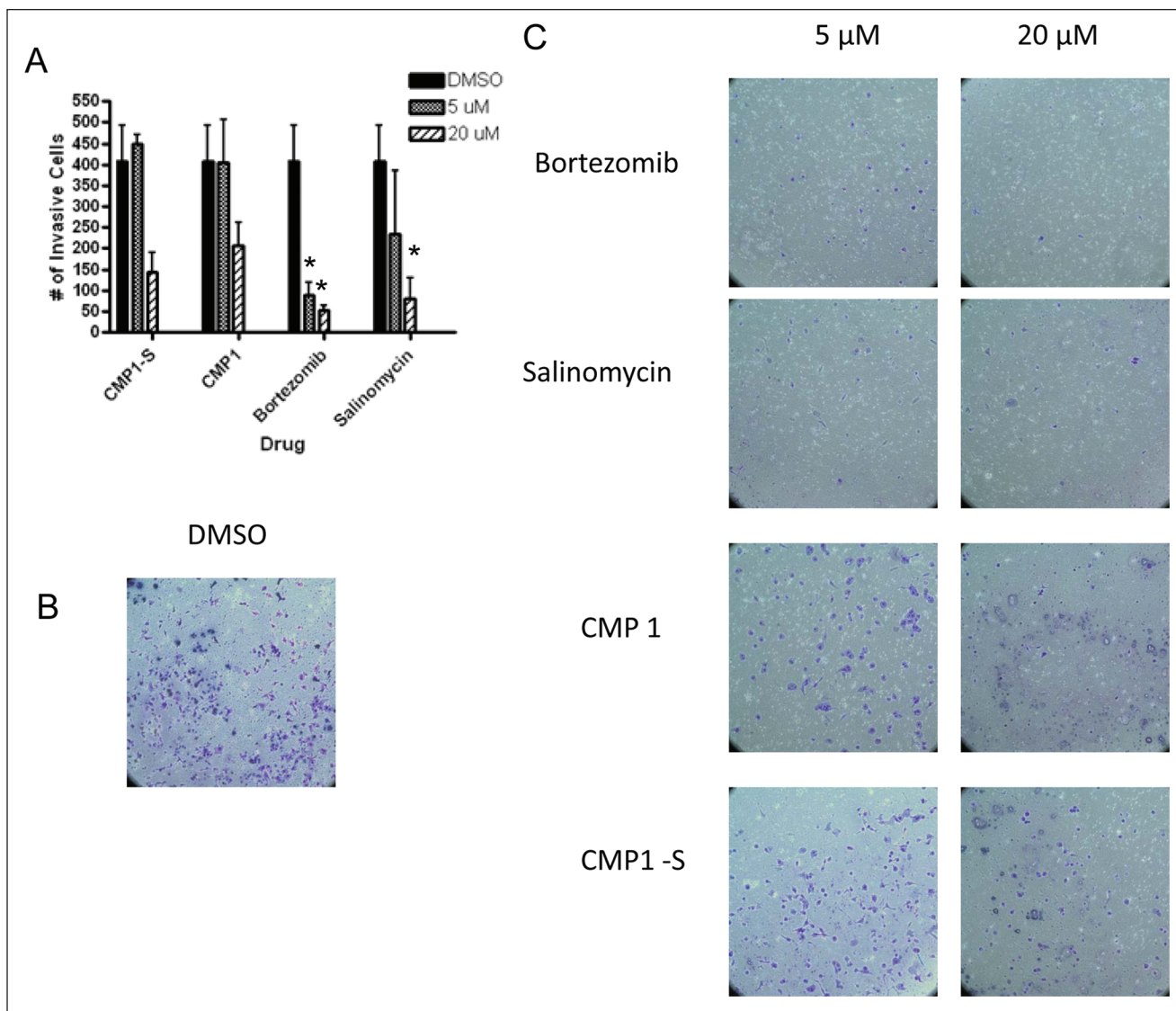


**Figure 4.** Results from the PANCI Matrigel cell invasion assay. PANCI cells were allowed to invade Matrigel membrane toward stem cell media (SCM) for 24 h and then fixed and stained. Two independent experiments were performed and averaged to generate error bars. \*Indicates statistical significance compared with DMSO using a pairwise Student *t* test ( $p < 0.05$ ). (A) Bar graph of effect of compounds on PANCI cell migration assay. (B) Bright-field images at 10 $\times$  of cells treated with DMSO. (C) Bright-field images of cells treated with bortezomib, salinomycin, CMP1, and compound with similar function to CMP1 (CMP1-S), all tested at 5 and 20  $\mu$ M in the invasion assay. Cells were stained with the Diff Quick staining kit (Dade Behring, Newark, DE) and counted.

pancreatic cancer, pancreatic CSCs are highly resistant to treatment,<sup>18</sup> and our results suggest that pancreatic cells are quite resistant to this drug, further supporting the need for additional novel treatments.

#### *A Secondary Functional CSC Matrigel Invasion Assay to Test Compounds Identified in the Primary Proliferation Assay*

To determine whether the compounds selected from the proliferation assay could also inhibit the invasive ability of

CSCs, a Matrigel invasion assay was used as a secondary assay (Fig. 4). In this assay, cells migrate toward the SCM media, and after 24 h under cell culture conditions, the noninvasive cells are removed and the invasive cells are fixed, stained, and counted.<sup>24,25</sup> The noninvasive cells are removed prior to staining to determine viability and to demonstrate negligence permeability of the compounds across the matrix (data not shown). Compared with DMSO (Fig. 4B), bortezomib (Fig. 4C) and salinomycin (Fig. 4C) were able to significantly inhibit invasion at both the lower and higher concentrations tested (Fig. 4A). At the higher concentration, CMP1 (Fig. 4C) and CMP1-S, a compound

inhibiting the same target (**Fig. 4C**), were both able to inhibit invasion toward the SCM (**Fig. 4A**), demonstrating that the proliferation-based assay used for primary screening had the ability to select for compounds capable of inhibiting the invasive ability of CSCs.

### A High-Content–Based NANOG-GFP Assay for Measuring “Stemness” of CSCs

A possible mechanism by which compounds could reduce resistant CSCs to treatment is by modulating their stem cell–like characteristics. To determine the ability of the compounds to regulate the stem cell–like properties of CSCs, we used a high-content imaging assay using a 4T1.2 mouse breast cancer cells with a Nanog-GFP reporter. In the growth conditions used, about 30% to 40% of the 4T1.2 Nanog-GFP cells are GFP+, demonstrating they express Nanog (Thomas Sayers Laboratory–NCI Frederick, unpublished data). If the GFP+ cells are then sorted and placed back in culture, the same percentage of cells will remain GFP+ and are much more metastatic when seeded in an animal (Thomas Sayers Laboratory–NCI Frederick, unpublished data). The selection of Nanog as a marker for CSCs was based on literature supporting the role of this gene in maintaining the CSCs phenotype.<sup>26–30</sup> To analyze the GFP content in the 4T1.2 cells after compound treatment, we fixed cells and stained the nuclei with Hoechst dye to determine cell number. A nuclear-masked–based compartmentalization algorithm was used to measure nuclear GFP signal from each cell. A mean average nuclear GFP signal per cell for each compound treatment was computed by averaging the nuclear GFP signal from each cell counted in a well. Data were normalized to DMSO-treated cells. 67 compounds reduced cell number to  $\leq 30\%$  (similar cutoff used for the cell proliferation assay), including the two pan-active hits identified using the % viability method and the five pan-active hits found from the CRC method (data not shown). When analyzing the data from the Nanog channel by looking at average GFP expression per cell, very few compounds effectively reduced the mean nuclear Nanog-GFP signal per cell. **Figure 5A** shows a dose-response profile from a compound (CMP4) that is able to reduce both the Nanog-dependent GFP signal per cell and the signal in the Hoechst channel. The images for three different concentrations of CMP4 treatment in both channels are shown in **Figure 5B**. CMP1, a compound selected as a pan-active hit from the % viability analysis, shows a decrease in cell viability with an increase in mean nuclear GFP signal per cell before no signal is detected at high compound doses because no cells survive the treatment. When further analyzing the images, it can be observed that the majority of the cells are dying with compound treatment (**Fig. 5C,D**), but the few surviving cells are high expressers of Nanog (**Fig. 5C,D**). We currently do not have an explana-

tion for this effect, and it is under investigation that these surviving cells could be drug-resistant cells that still remain alive albeit with treatment.

### Discussion

Reports of the drug-resistant nature of CSCs prompted our lab to design assays that could be used to screen for compounds that inhibit the growth of these very aggressive cancer cells. We chose to investigate the CSC models of prostate cancer and pancreatic cancer because of the limited treatments currently available for advanced stages of these two diseases and their highly lethal metastatic nature. CSC populations in an HTS setting are challenging because of the difficulty to isolate and scale up cell production. As previously mentioned, these cells are commonly isolated using FACS for certain cell adhesion proteins such as CD44, CD24, or CD133. Adapting this method of CSC isolation to produce enough cells to conduct an HTS assay is not practical because of the cost of the antibodies and also the time required to sort the millions of cells needed. To date, because of these constraints, very few HTS assays have been performed using CSCs. A previously published study described an HTS assay that used CSCs generated from highly transformed cells called HMLER breast cancer cells.<sup>23</sup> These cells were transformed to have a mesenchymal phenotype (a hallmark of CSCs) by downregulation of E-cadherin, producing expression of high levels of CD44 and low levels of CD24.<sup>23</sup> This screen identified salinomycin as a CSC cytotoxic compound. Our approach was to generate CSCs using the spheroid technique and develop a cell growth assay in a 1536-well microplate format to screen for compounds that are cytotoxic against these highly aggressive CSCs. The spheroid technique affords for the production of large amounts of CSCs and therefore enables the availability of these cells for the use in HTS without the need to engineer the cells.

To validate the design of our CellTiter-Glo–based proliferation assay, we first examined the effects of salinomycin, the compound identified in the CSCs screen with HMLER cells. Previous studies have demonstrated that this compound is effective at inducing apoptosis in prostate cancer cells and interferes with the end-stage progression of hormone-indifferent and chemotherapy-resistant prostate cancer.<sup>31</sup> Importantly, nonmalignant RWPE-1 prostate cells were relatively less sensitive to salinomycin-induced lethality.<sup>31</sup> In pancreatic cancer, it was recently shown that in combination with the standard-of-care gemcitabine, which targets non-CSCs, salinomycin inhibited the growth of pancreatic cancer cells in vitro and in vivo by inhibiting the growth of CD133+ or side-population isolated CSCs.<sup>32</sup> In both of our CSC models, salinomycin was able to effectively, reproducibly, and significantly inhibit their growth in a 1536-well microplate format. A second positive control



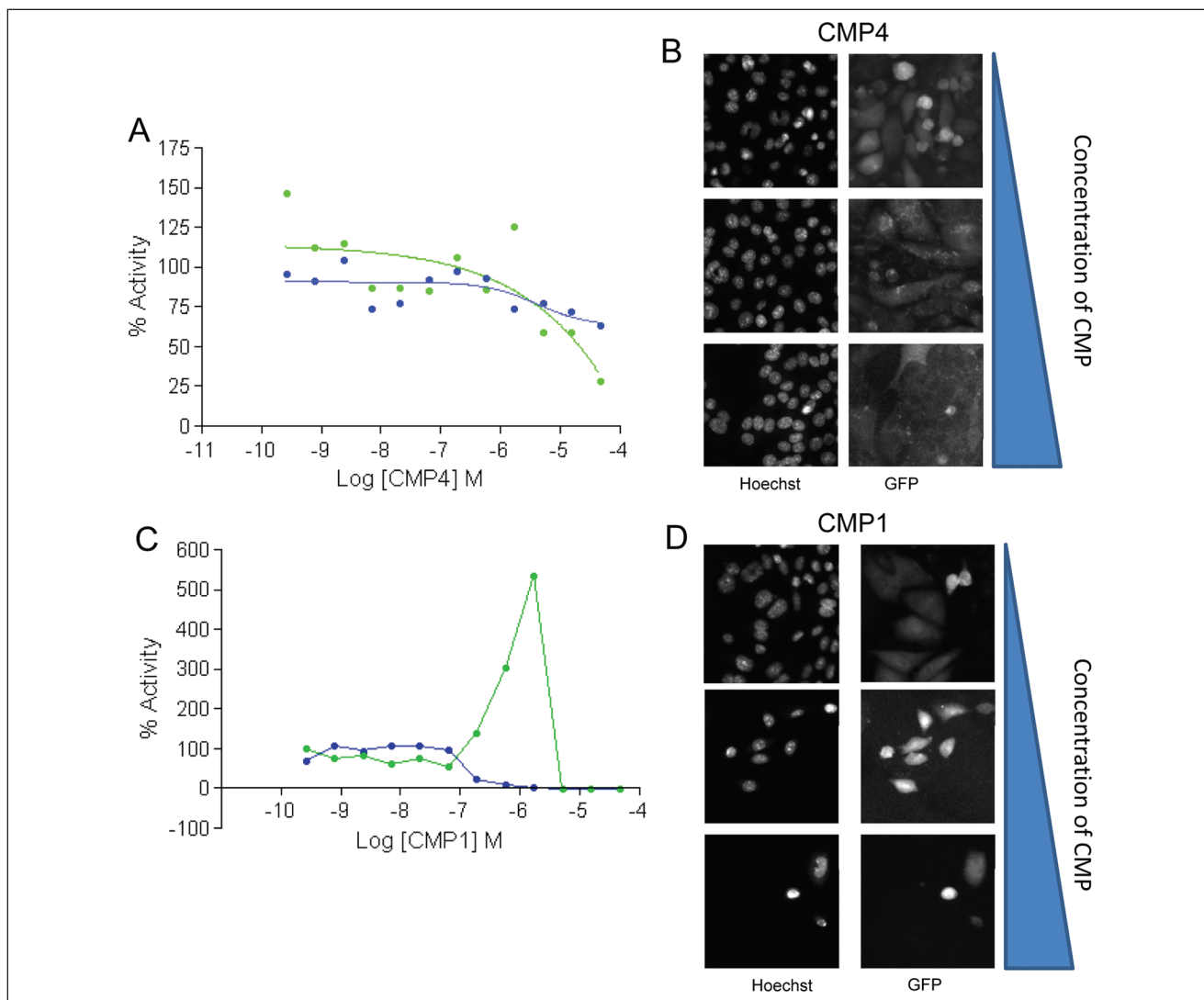


**Figure 5.** Results from the 4T1.2 Nanog-GFP reporting imaging assay. **(A)** Dose-response curves of CMP4 in the 4T1.2 Nanog-GFP cells measured using the ArrayScan (Thermo Scientific, Fisher Scientific, Fair Lawn, NJ). The overall cell viability was measured using Hoechst staining (blue) to assess nuclear count, and mean nuclear Nanog-GFP signal per cell is also shown (green). Percent activity compared with DMSO control-treated cells appears on the y-axis and the log molar concentration on the x-axis. **(B)** Fluorescent 20 $\times$  images from the high-content screen (HCS) demonstrate a decrease in both nuclear count and average nuclear Nanog-GFP signal per cell with increasing concentrations of CMP4. **(C)** Dose-response curve for CMP1 in Nanog-GFP cells demonstrating a decrease in cell viability by nuclear count yet an increase in mean nuclear Nanog-GFP signal per cell expression in surviving cells before no signal is detected at higher doses when there are no surviving cells. Percent activity compared with DMSO control-treated cells appears on the y-axis and the log molar concentration on the x-axis. **(D)** Fluorescent 20 $\times$  images from the HCS assay demonstrate a decrease in nuclear count and yet an increase in total Nanog-GFP expression per cell with increasing concentrations of CMP1.

that we employed was the protease inhibitor bortezomib based on personal communication that it was quite effective at inhibiting the growth of mouse breast CSCs (unpublished results from Thomas Sayers Laboratory). In both systems, bortezomib was very effective at inhibiting growth of not only the adherent cells but also the spheroid-derived populations. Unfortunately, although bortezomib appears *in vitro* as a very promising treatment for pancreatic cancer, when

tested *in vivo* in a mouse orthotopic model of pancreatic adenocarcinoma, it was ineffective, further demonstrating the need for new compounds that attack this deadly disease.<sup>33</sup>

The 1536-microplate spheroid-derived CSC growth assay was used to screen an in-house small-molecule collection consisting of 112 compounds targeting oncology-relevant pathways/mechanisms of survival, also referred to

as the Mechanism Interrogation PlatE or MIPE plate. This library includes approved chemotherapeutics, preclinical candidates, compounds in different phases of clinical development, and investigational compounds targeting key pathways and mechanism in oncology. This library includes known drugs with a long history of clinical use such as 5-fluorouracil and vincristine, as well as molecules in advanced clinical assessments that embody the contemporary approach of highly targeted enzyme and pathway inhibitors such as amuvatinib (DNA repair inhibitor) and talmapimod (p38 MAPK inhibitor). Because drug combinations can offer a better chance at providing high efficacy while reducing dose and potentially toxicity, molecules that failed in various phases of trials such as tozasertib (Aurora kinase inhibitor) and alvespimycin (HSP90 inhibitor) are also included. Recently disclosed clinical compounds targeting novel cellular targets relevant to the cancer types, including inhibitors of spleen tyrosine kinase (SYK), Bruton's tyrosine kinase (BTK), PKC $\gamma$ , MEK, HSP90, PARP, and PI(3)K, are also included in the collection. In addition, the library includes a degree of chemical diversity for each target to be able to explore compound activity differences associated with varying selectivity profiles. For example, many epidermal growth factor receptor (EGFR) inhibitors are included—gefitinib, lapatinib, neratinib, and dacomitinib—to help determine target versus compound-based activity. The composition of this collection allows us to potentially find drugs that can be efficiently used to treat CSCs, as well as to find biological information on what pathways are relevant for the survival of CSCs.

The results from the screen of this collection suggest that the major driver of cellular survival to the compounds tested is not necessarily the differentiation state of the cells but rather the cancer type. Although there might be a small trend toward CSCs being more resistant than the parental adherent cells, which are more differentiated, in general, the difference in compounds' cytotoxic effect between LNCaP and PANC1 cells is larger than between spheres and adherent cells. However, two compounds were identified using the % viability criteria that inhibited growth of both spheres and adherent cells from both the LNCaP and PANC1 cells (Suppl. Fig. S2). This perhaps unexpected result suggests that overall CSCs are not significantly more resistant than adherent cells in an *in vitro* experimental setting when solely looking at % viability but that the previously observed resistance seen *in vivo* might be due to effects of the tumor environment (drug accessibility, presence of drug transporters, and effects of the tumor niche on CSCs).<sup>22</sup> It also suggests that perhaps assays where the cytotoxic effect of compounds on CSCs is measured in a true 3D spheroid environment may be more relevant than a nonadherent 2D CSC growth assay of the type used here. More complex assays that contain additional cell types and the presence of

extracellular matrix are under intense investigation and development in the drug discovery arena for this reason.

When applying the CRC hit selection method, five compounds were shown to be pan-active against both cell lines and growth conditions, with only one compound overlapping between the two analysis methodologies, CMP2 (Suppl. Table S3). The IC<sub>50</sub> values for these compounds varied, but overall it was commonly found that the IC<sub>50</sub> required to kill to the spheroid-based cells was 3-fold higher than the adherent populations. Further investigation of these active compounds determined that they included compound CMP2, which was nonselective; compound CMP1, which was PANC1 selective; and CMP3, which was LNCaP selective (Fig. 3A–C, respectively). In addition, CMP1 and a compound with a similar mechanism of action, CMP1-S, were further tested in a functional assay of CSC invasion using Matrigel-coated Boyden chambers. It is thought that the aggressive nature of CSCs occurs because they are the most invasive cells and are able to survive and metastasize to other vital organs, leading to fatality in patients.<sup>2–4</sup> Previous work using the same prostate and pancreatic cancer cell lines used here demonstrates that these highly invasive cells have a stem-like phenotype,<sup>17</sup> have undergone an epithelial to mesenchymal transition (EMT) during the process of invasion, and are also highly tumorigenic when injected into mice.<sup>17,18</sup> In addition to the positive controls salinomycin and bortezomib, both CMP1 and CMP1-S prevented the invasion of CSCs (Fig. 4). Compounds that are able to inhibit the invasion of CSCs toward SCM are more likely to be effective at blocking tumor formation in mouse models of CSCs. As previously demonstrated, concentrations higher than the IC<sub>50</sub> values derived from the cell proliferation assay were tested since much higher concentrations are needed to inhibit invasion through the extracellular matrix composed of Matrigel toward stem cell media.<sup>17,18</sup> Additional studies will be carried out expanding the doses tested in the invasion assays to determine the concentrations required to inhibit invasion toward SCM.

The MIPE compounds were also tested for their ability to regulate the stem cell state in CSCs as a potential mechanism for compounds to reduce resistance of these cells to cytotoxic agents. The Nanog gene regulates the stem cell state in embryonic stem cells and has been recently identified as a key regulator of CSCs in many systems, including prostate, pancreas, and breast.<sup>26–30</sup> These cells were originally derived from a spontaneous metastatic carcinoma found in a BALB/cfC2H mouse and termed the 4T1 cell line.<sup>34</sup> Further single-cell cloning led to the development of a highly aggressive line, 4T1.2, which metastasizes to bone, lungs, and other sites in the animal. The 4T1 model was also used in the aforementioned HMLER screen to confirm effective inhibition of metastasis formation with the hits identified in their screen. Using a highly aggressive mouse breast cancer cell line 4T1.2 that has been stably infected

with a Nanog-GFP reporter as a model system allowed us to screen the MIPE library with high-content technology in addition to the luminescent cell proliferation assay we developed. Unlike the prostate and pancreatic models of CSCs, this model is well established to visualize the effects compounds have on primary tumor formation as well as the appearance of metastases<sup>34,35</sup> and is primarily why we selected it to screen using high-content imaging. Screening using a mixed population of cells is inherently difficult, and the majority of the data demonstrated that compounds were cytotoxic to these cells, positive or negative for GFP, as measured by reduced cell number. As mentioned above, this bias could be attributed to the fact that the library we screened contains oncology-based compounds that mainly target cancer cells by inducing cytotoxicity. Screening with additional libraries may remove this bias when using a high-content approach. Interestingly, for the top pan-active compounds selected from the cell proliferation assay, the mean nuclear Nanog-GFP signal per cell actually increased at high doses before no signal could be detected at those very high doses where there were no surviving cells in the well. **Figure 5C,D** shows the effect of CMP1 on the Nanog-GFP imaging assay. The images show how cells surviving treatment with CMP1 had very high Nanog expression. The heterogeneity of the 4T1.2-Nanog cells and types of compounds we are looking for is not well suited for an HTS assay using high-content imaging. However, by having both sets of data from the cytotoxicity assay and Nanog-GFP assay, one can begin to appreciate the value of the high-content set and the additional information it can provide about the biology of certain compounds. Finally, a few compounds actually increased the expression of Nanog without affecting nuclear count, and they will be followed up as potential CSC activators in our lab.

In conclusion, the research presented here demonstrates one of the first qHTS-based assays using true, nonengineered CSCs. The cell growth assay developed is a very sensitive and can be used to screen additional libraries with different types of CSCs in the future. In addition, we tested the MIPE library against mouse breast cells stably expressing a marker of stemness, Nanog. This assay proved to be quite heterogeneous and, similar to the proliferation assay, found hits resulting in cytotoxicity using the Hoechst nuclear staining channel irrespective of Nanog expression. Although this article focuses on selection of pan-active compounds, we are also pursuing compounds that are selective for cells from each cancer type. We are also planning to screen this cell proliferation assay with additional libraries of compounds as single agents and in combinations to determine which pathways need to be inhibited to produce complete toxicity against CSCs. We believe this will result in the development of novel therapies for aggressive forms of cancer and will specifically result in targeting metastasis and recurrence.

## Acknowledgments

We thank Matthew Boxer, Damien Duveau, Christopher Leclair, and Jian-kang Jiang of NCATS for their assistance with acquiring the compounds for the MIPE library.

## Declaration of Conflicting Interests

The authors declared no potential conflicts of interest with respect to the research, authorship, and/or publication of this article confirmed statement is accurate.

## Funding

The authors disclosed receipt of the following financial support for the research, authorship, and/or publication of this article: This research was partly supported by the NIH Common Fund Molecular Libraries and Imaging Program, grant U54 MH084681. In addition, this project has been funded in part with federal funds from the Frederick National Laboratory for Cancer Research, National Institutes of Health, under contract HHSN261200800001E. The content of this publication does not necessarily reflect the views or policies of the Department of Health and Human Services, nor does mention of trade names, commercial products, or organizations imply endorsement by the U.S. government.

## References

1. Jemal, A.; Siegel, R. *Cancer Facts and Figures*; American Cancer Society: Atlanta, GA, **2011**.
2. Moss, R. A.; Lee, C. Current and Emerging Therapies for the Treatment of Pancreatic Cancer. *Oncol. Targets Ther.* **2010**, *3*, 111–127.
3. Shah, A. N.; Summy, J. M.; Zhang, J.; Park, S. I.; Parikh, N. U.; Gallick, G. E. Development and Characterization of Gemcitabine-Resistant Pancreatic Tumor Cells. *Ann. Surg. Oncol.* **2007**, *14*(12), 3629–3637.
4. Ischenko, I.; Seeliger, H.; Jauch, K. W.; Bruns, C. J. Metastatic Activity and Chemotherapy Resistance in Human Pancreatic Cancer—Influence of Cancer Stem Cells. *Surgery* **2009**, *146*(3), 430–434.
5. Merl, M. Y.; Li, J.; Saif, M. W. The First-Line Treatment for Advanced Pancreatic Cancer. Highlights from the “2010 ASCO Gastrointestinal Cancers Symposium.” Orlando, FL, USA. January 22–24, 2010. *Jop* **2010**, *11*(2), 148–150.
6. Crea, F.; Duhagon Serrat, M. A.; Hurt, E. M.; Thomas, S. B.; Danesi, R.; Farrar, W. L. BMI1 Silencing Enhances Docetaxel Activity and Impairs Antioxidant Response in Prostate Cancer. *Int. J. Cancer* **2010**, *128*(8), 1946–1954.
7. O'Brien, C. A.; Kreso, A.; Jamieson, C. H. Cancer Stem Cells and Self-renewal. *Clin. Cancer Res.* **2010**, *16*(12), 3113–3120.
8. Sengupta, A.; Cancelas, J. A. Cancer Stem Cells: A Stride towards Cancer Cure? *J. Cell Physiol.* **2010**, *225*(1), 7–14.
9. Reiman, J. M.; Knutson, K. L.; Radisky, D. C. Immune Promotion of Epithelial-Mesenchymal Transition and Generation of Breast Cancer Stem Cells. *Cancer Res.* **2010**, *70*(8), 3005–3008.

10. Raimondi, C.; Gianni, W.; Cortesi, E.; Gazzaniga, P. Cancer Stem Cells and Epithelial- Mesenchymal Transition: Revisiting Minimal Residual Disease. *Curr. Cancer Drug Targets* **2010**, *10*(5), 496–508.
11. Bhattacharyya, S.; Khanduja, K. L. New Hope in the Horizon: Cancer Stem Cells. *Acta Biochim. Biophys. Sin. (Shanghai)* **2010**, *42*(4), 237–242.
12. Li, C.; Heidt, D. G.; Dalerba, P.; Burant, C. F.; Zhang, L.; Adsay, V.; Wicha, M.; Clarke, M. F.; Simeone, D. M. Identification of Pancreatic Cancer Stem Cells. *Cancer Res.* **2007**, *67*(3), 1030–1037.
13. Dontu, G.; Abdallah, W. M.; Foley, J. M.; Jackson, K. W.; Clarke, M. F.; Kawamura, M. J.; Wicha, M. S. In Vitro Propagation and Transcriptional Profiling of Human Mammary Stem/Progenitor Cells. *Genes Dev.* **2003**, *17*(10), 1253–1270.
14. Hurt, E. M.; Kawasaki, B. T.; Klarmann, G. J.; Thomas, S. B.; Farrar, W. L. CD44+ CD24(–) Prostate Cells Are Early Cancer Progenitor/Stem Cells That Provide a Model for Patients with Poor Prognosis. *Br. J. Cancer* **2008**, *98*(4), 756–765.
15. Gaviraghi, M.; Tunici, P.; Valensin, S.; Rossi, M.; Giordano, C.; Magnoni, L.; Dandrea, M.; Montagna, L.; Ritelli, R.; Scarpa, A.; et al. Pancreatic Cancer Spheres Are More Than Just Aggregates of Stem Marker Positive Cells. *Biosci. Rep.* **2010**, *31*(1), 45–55.
16. Gou, S.; Liu, T.; Wang, C.; Yin, T.; Li, K.; Yang, M.; Zhou, J. Establishment of Clonal Colony-Forming Assay for Propagation of Pancreatic Cancer Cells with Stem Cell Properties. *Pancreas* **2007**, *34*(4), 429–435.
17. Klarmann, G. J.; Hurt, E. M.; Mathews, L. A.; Zhang, X.; Duhagon, M. A.; Mistree, T.; Thomas, S. B.; Farrar, W. L. Invasive Prostate Cancer Cells Are Tumor Initiating Cells That Have a Stem Cell–Like Genomic Signature. *Clin. Exp. Metastasis* **2009**, *26*(5), 433–436.
18. Mathews, L. A.; Cabarcas, S. M.; Hurt, E. M.; Zhang, X.; Jaffee, E. M.; Farrar, W. L. Increased Expression of DNA Repair Genes in Invasive Human Pancreatic Cancer Cells. *Pancreas* **2011**, *40*(5), 730–739.
19. Duhagon, M. A.; Hurt, E. M.; Sotelo-Silveira, J. R.; Zhang, X.; Farrar, W. L. Genomic Profiling of Tumor Initiating Prostatospheres. *BMC Genomics* **2010**, *11*(324), 1–16.
20. Inglese, J.; Auld, D. S.; Jadhav, A.; Johnson, R. L.; Simeonov, A.; Yasgar, A.; Zheng, W.; Austin, C. P. Quantitative High-Throughput Screening: A Titration-Based Approach That Efficiently Identifies Biological Activities in Large Chemical Libraries. *Proc. Natl. Acad. Sci. U. S. A.* **2006**, *103*(31), 11473–11478.
21. Wang, Y.; Jadhav, A.; Southal, N.; Huang, R.; Nguyen, D. T. A Grid Algorithm for High Throughput Fitting of Dose-Response Curve Data. *Curr. Chem. Genomics* **2010**, *4*, 57–66.
22. Cabarcas, S. M.; Mathews, L. A.; Farrar, W. L. The Cancer Stem Cell Niche—There Goes the Neighborhood? *Int. J. Cancer* **2012**, *129*(10), 2315–2327.
23. Gupta, P. B.; Onder, T. T.; Jiang, G.; Tao, K.; Kuperwasser, C.; Weinberg, R. A.; Lander, E. S. Identification of Selective Inhibitors of Cancer Stem Cells by High-Throughput Screening. *Cell* **2009**, *138*(4), 645–659.
24. Crea, F.; Mathews, L. A.; Farrar, W. L.; Hurt, E. M. Targeting Prostate Cancer Stem Cells. *Anticancer Agents Med. Chem.* **2009**, *9*(10), 1105–1113.
25. Singh, A.; Settleman, J. EMT, Cancer Stem Cells and Drug Resistance: An Emerging Axis of Evil in the War on Cancer. *Oncogene* **2010**, *29*(34), 4741–4751.
26. Jeter, C. R.; Badeaux, M.; Choy, G.; Chandra, D.; Patrawala, L.; Liu, C.; Calhoun-Davis, T.; Zaehres, H.; Daley, G. Q.; Tang, D. G. Functional Evidence That the Self-renewal Gene NANOG Regulates Human Tumor Development. *Stem Cells* **2009**, *27*(5), 993–1005.
27. Jeter, C. R.; Liu, B.; Liu, X.; Chen, X.; Liu, C.; Calhoun-Davis, T.; Repass, J.; Zaehres, H.; Shen, J. J.; Tang, D. G. NANOG Promotes Cancer Stem Cell Characteristics and Prostate Cancer Resistance to Androgen Deprivation. *Oncogene* **2012**, *30*(36), 3833–3845.
28. Lu, Y. H.; Zhu, H.; Wang, Z. W.; Fan, X. J.; Zhu, S. J.; Li, X. H.; Wang, Y.; Lu, J. J.; Zhu, M. Y. Altered Expressions of Embryonic Stem-Related Genes in Pancreatic Cancer Stem Cell [in Chinese]. *Zhonghua Yi Xue Za Zhi* **2011**, *91*(44), 3107–3110.
29. Wen, J.; Park, J. Y.; Park, K. H.; Chung, H. W.; Bang, S.; Park, S. W.; Song, S. Y. Oct4 and Nanog Expression Is Associated with Early Stages of Pancreatic Carcinogenesis. *Pancreas* **2010**, *39*(5), 622–626.
30. Tang, S. N.; Fu, J.; Nall, D.; Rodova, M.; Shankar, S.; Srivastava, R. K. Inhibition of Sonic Hedgehog Pathway and Pluripotency Maintaining Factors Regulate Human Pancreatic Cancer Stem Cell Characteristics. *Int. J. Cancer* **2012**, *131*(1), 30–40.
31. Kim, K. Y.; Yu, S. N.; Lee, S. Y.; Chun, S. S.; Choi, Y. L.; Park, Y. M.; Song, C. S.; Chatterjee, B.; Ahn, S. C. Salinomycin-Induced Apoptosis of Human Prostate Cancer Cells Due to Accumulated Reactive Oxygen Species and Mitochondrial Membrane Depolarization. *Biochem. Biophys. Res. Commun.* **2011**, *413*(1), 80–86.
32. Zhang, G. N.; Liang, Y.; Zhou, L. J.; Chen, S. P.; Chen, G.; Zhang, T. P.; Kang, T.; Zhao, Y. P. Combination of Salinomycin and Gemcitabine Eliminates Pancreatic Cancer Cells. *Cancer Lett.* **2011**, *313*(2), 137–144.
33. Marten, A.; Zeiss, N.; Serba, S.; Mehrle, S.; von Lilienfeld-Toal, M.; Schmidt, J. Bortezomib Is Ineffective in an Orthotopic Mouse Model of Pancreatic Adenocarcinoma. *Mol. Cancer Ther.* **2008**, *7*(11), 3624–3631.
34. Lelekakis, M.; Moseley, J. M.; Martin, T. J.; Hards, D.; Williams, E.; Ho, P.; Lowen, D.; Javni, J.; Miller, F. R.; Slavin, J.; et al. A Novel Orthotopic Model of Breast Cancer Metastasis to Bone. *Clin. Exp. Metastasis* **1999**, *17*(2), 163–170.
35. Bolin, C. M.; Sutherland, C.; Tawara, K.; Moselhy, J.; Jorecyk, C. L. Novel Mouse Mammary Cell Lines for In Vivo Bioluminescence Imaging (BLI) of Bone Metastasis. *Biol. Proced. Online* **2012**, *14*(1), 1–6.